

# Morphology and viscoelastic behavior of silicone rubber/EPDM/Cloisite 15A nanocomposites based on Maxwell model

Leila Bazli<sup>1</sup> · Alireza Khavandi<sup>1</sup> · Mohammad Ali Boutorabi<sup>1,2</sup> · Mohammad Karrabi<sup>3</sup>

Received: 10 May 2016 / Accepted: 16 August 2016 / Published online: 26 September 2016  
© Iran Polymer and Petrochemical Institute 2016

**Abstract** Blends of silicone rubber (SR) and ethylene propylene diene monomer (EPDM) are immiscible due to different polarity and poor interfacial surface tension between their rubber chains. In this study, compatibilizing effect of a nanoclay addition in SR/EPDM blends was investigated. Viscoelasticity and morphology of nanocomposites based on SR and EPDM, containing 10, 20 and 30 wt% of EPDM and 3, 6 and 9 phr of nanoclay (Cloisite 15A), were studied. The curing behavior of the samples showed that the vulcanization rate and cross-link density of the blends increased with increases in SR content. Morphological study was conducted by XRD, SEM and EDX analyses and they indicated that the nanoparticles tended to disperse in the EPDM phase and consequently caused hardness and the elasticity of this phase in nanocomposites increased. Tensile properties of the samples showed a good fitting between that of experiments and the Maxwell model at initial time of testing (1.5 s) for all the blends. Sample parameters including modulus ( $E$ ), viscosity ( $\eta$ ) and relaxation time ( $\tau$ ) calculated by the Maxwell model revealed that those samples with higher content of nanoparticles exhibit higher modulus and lower relaxation time. The good match in tensile properties based on Maxwell model and those of

the experimental data was attributed to good dispersion of nanoclay in the blends.

**Keywords** SR · EPDM · Nanocomposite · Morphological study · Maxwell model

## Introduction

In recent decades, clay has been used as a promising filler to produce rubber blend nanocomposites [1–3]. These layered silicates have high negative surface charge, which prevent the dispersion of nanolayers in polymer matrices due to incompatibility between the hydrophobic polymer chains and hydrophilic layered silicates. The replacement of inorganic cations in the intergalleries of silicates by organic cations can increase intergallery spacing [4–6] which, in turn, can improve the properties of nanocomposite due to intercalation or exfoliation of silicate layers in the matrix [7–9].

Because of having the ability to customize and combine the attractive properties of the components in the blend in a cheap way, rubber blends are widely used in different applications [10–12]. The properties of such polymer blends depend on the morphology (co-continuous or matrix-dispersed structure) besides their individual component properties. Co-continuous morphology can result in a more effective combination of the components' properties. Thus, we can influence the final blend properties by controlling the morphology through variation in composition, elasticity, viscosity ratio and the interfacial tension between two polymers [13–15]. Due to the capability of nanoclays for improving morphological, mechanical and thermal properties of polymers, research works have been developed on rubber/organoclay nanocomposites using different rubbers

✉ Mohammad Karrabi  
m.karabi@ippi.ac.ir

<sup>1</sup> School of Metallurgy and Materials Engineering, Iran University of Science and Technology (IUST), Narmak, Tehran, Iran

<sup>2</sup> Center of Excellence for High Strength Alloys Technology (CEHSAT), Tehran, Iran

<sup>3</sup> Rubber Group, Iran Polymer and Petrochemical Institute, Nano and Smart Polymers Center of Excellence, Tehran, Iran

and by a variety of methods such as solution mixing and melt mixing [16–18].

Polymeric insulating materials are used in various electrical equipment for their superior service properties against pollution, high electrical parameters, lighter weight and improved seismic performance [19–21]. Silicone rubbers (SR) are widely used in insulation applications for their good properties at low and high temperatures, high oxidation resistance and good hydrophobicity [22–24]. Ethylene propylene diene monomers (EPDM) also possess good mechanical properties, heat aging resistance, chemical resistance and dielectric properties. This combination of properties has attracted the attention of researchers to develop suitable blends of these elastomers [23, 25, 26].

In this study, SR/EPDM/clay nanocomposites were prepared at different compositions using a laboratory two-roll mill. Characterization of the samples morphology was carried out by X-ray diffractometry (XRD), scanning electron microscopy (SEM) and energy dispersive X-ray spectroscopy (EDX). In addition, the variations in mechanical, dynamic mechanical and cure properties were investigated. Dynamic mechanical thermal analysis is a test method for measuring the viscoelastic parameters as a function of temperature [27]. This technique is highly sensitive for detecting the changes in internal molecular mobility and morphology [28].

The preferential location of the clay particles in the polymer blend has been estimated based on the difference between the interfacial tensions of the components. Among several approaches made to determine the interfacial tension between two components, two approaches are more common for polar systems [29–31].

The first is the geometric mean equation, as follows:

$$\gamma_{AB} = \gamma_A + \gamma_B - 2 \left( \left( \gamma_A^D \gamma_B^D \right)^{1/2} + \left( \gamma_A^P \gamma_B^P \right)^{1/2} \right), \quad (1)$$

The second is Wu's harmonic mean equation:

$$\gamma_{AB} = \gamma_A + \gamma_B - 4 \left( \frac{\gamma_A^D \gamma_B^D}{\gamma_A^D + \gamma_B^D} + \frac{\gamma_A^P \gamma_B^P}{\gamma_A^P + \gamma_B^P} \right). \quad (2)$$

In these equations, subscripts *A* and *B* stand for polymeric components, and  $\gamma$  is the surface tension. Superscripts *P* and *D* reveal the dispersive and polar parts of the surface tension, respectively, and the relation between  $\gamma_i^P$  and  $\gamma_i^D$  is as follow:

$$\gamma_i = \gamma_i^P + \gamma_i^D. \quad (3)$$

In this study, the surface tensions at room temperature for SR (polydimethylsiloxane), EPDM and clay were extrapolated to the processing temperature (50 °C) using the temperature coefficients ( $-d\gamma/dT$ ) according to data in the literature.

Some papers discuss the viscoelastic behavior of rubber and predict their properties based on viscoelastic models [32]. In the present investigation, stress–strain curves of the nanocomposites at the initial time of deformation were modeled using Maxwell model (Eq. 4) [33],

$$\varepsilon^\circ = \frac{1}{E} \sigma^\circ + \frac{1}{\eta} \dot{\sigma}. \quad (4)$$

## Experimental

### Materials

Silicone rubber (SR), HD-9170 (vinyl methyl-based silicone; density: 1.18 g/cm<sup>3</sup> and hardness: 70 Shore A) was supplied by Hongda Co., Ltd., (China). EPDM grade KEP 270 (ML (1 + 4) = 70 at 125 °C; ethylene content = 57.0 %; ethylene norbornene content = 4.5 % and density = 0.86 g/cm<sup>3</sup>) was produced by Kumho Polychem Co., Ltd., (Korea). Peroxide curing agent, DCP (dicumyl peroxide with 98 % purity) obtained from Hercules Incorporated (USA). Nanoclay (Cloisite 15A) was purchased from Southern Clay (USA).

### Sample preparation

SR/EPDM/Cloisite 15A nanocomposites were mixed using a two-roll mill (Polymix 200L, Schwabenthan, Germany) as a mixer for 10 min at temperature of 50 °C. For preparation of the nanocomposite samples, at first the rubber bales were masticated for 3 min, then Cloisite 15A of different contents (3, 6, and 9 phr) were added and mixed for 3 min, and finally 1 phr of DCP was added into the mixer during 2 min with the rotor speed of 15 rpm and friction ratio of 1.6. The sample codes and the compositions of nanocomposites are listed in Table 1. Curing of samples was carried out by a hot hydraulic press of 100 ton, Bucher, Switzerland at temperature of 160 °C for 15 min. Thereafter, the cured samples underwent post-curing at 150 °C in an air-circulating oven for 2 h.

Before performing the tests, the prepared samples were stored for 24 h at room temperature to relax the shear stresses induced during mixing.

### Characterization

#### Frequency sweep test and curing behavior

Frequency sweep test of selected samples was performed at 50 °C in the range of 0.18–200 rad/s and in a constant strain of 7 % and cure rheometry of samples was investigated according to ASTM D2084 at 160 °C using a rubber processability analyzer (RPA2000™, Alpha Technologies, USA) with a bi-conical moving die.

**Table 1** Composition of the samples

Sample code	SR (phr)	EPDM (phr)	Cloisite 15A (phr)
E100C0	–	100	0
E100C3	–	100	3
E100C6	–	100	6
E100C9	–	100	9
Q100C0	100	–	0
Q100C3	100	–	3
Q100C6	100	–	6
Q100C9	100	–	9
Q90E10C0	90	10	0
Q90E10C3	90	10	3
Q90E10C6	90	10	6
Q90E10C9	90	10	9
Q80E20C0	80	20	0
Q80E20C3	80	20	3
Q80E20C6	80	20	6
Q80E20C9	80	20	9
Q70E30C0	70	30	0
Q70E30C3	70	30	3
Q70E30C6	70	30	6
Q70E30C9	70	30	9

All the samples were cured by 1 phr of DCP

### Morphological study of fractured surface

A Siemens X-ray diffraction (XRD D5000, Germany) was employed to study the distribution of nanoclay in the polymer matrix at room temperature. The changes in the gallery distances of the clay particles were measured within the range of  $2\theta = 2^\circ\text{--}10^\circ$  using Cu K $\alpha$  radiation ( $\lambda = 1.540598 \text{ \AA}$ ), operating at 40 kV and 40 mA with scanning rate of  $0.1^\circ/\text{min}$ .

Scanning electron microscopy (SEM) micrographs were acquired from cryo-fractured cross-sections of the specimens using VEGA, TESCAN of Czech Republic. The fracture surfaces were gold-coated before observation by SEM. In addition, energy dispersive X-ray spectroscopy (EDX) was carried out to obtain more evidence on the location of clay in the nanocomposites.

### Mechanical properties

Tensile strength and elongation-at-break of the nanocomposites were tested at room temperature from the dumb-bell-shaped specimens punched out from the compression-molded sheets. Tensile test was carried out according to ASTM D412 using Hiwa model 200, Iran. The crosshead speed was 500 mm/min. Measuring the hardness (Shore A) of nanocomposites was conducted as per ASTM D2240 by Zwick, Germany.

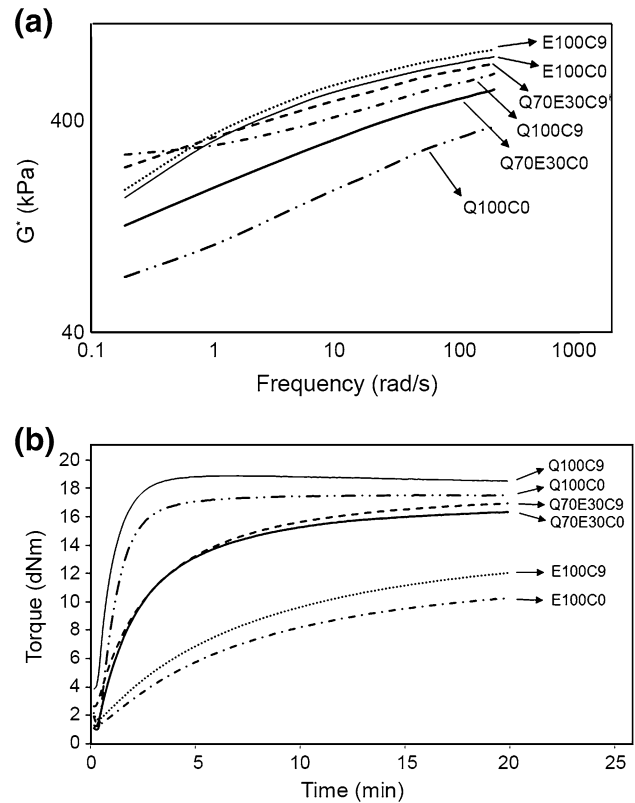


**Fig. 1** RPA test: **a** frequency sweep; and **b** cure rheometry

### Dynamic mechanical thermal analysis (DMTA)

Dynamic mechanical properties were evaluated using a dynamic mechanical analyzer in single cantilever bending  $100^\circ\text{C}$  at a heating rate of  $5^\circ\text{C}/\text{min}$  by Tritec 2000, DMTA-Triton, England.

## Results and discussion

### Viscoelastic behavior before and during cure stage

The variation of viscoelastic properties versus frequency for uncured samples was studied by frequency sweep test. As shown in Fig. 1a, before curing, the complex modulus of EPDM is higher than that of SR compounds because of high elasticity of EPDM at  $50^\circ\text{C}$ , also after adding the nanoclay, as expected, the complex modulus of the samples is increased. Comparing the behavior of E100C0 and E100C9 indicates that they are slightly different because of high elasticity of EPDM. Nevertheless, the presence of nanoclay in the SR-based samples shows stronger effect on complex modulus in comparison with the EPDM-based samples. As seen in Fig. 1a, a plateau region emerges at low frequencies for Q100C9, which is an evidence of rubber–filler network

**Table 2** Cure properties of the samples

Sample code	$t_2$ (min)	$t_{90}$ (min)	$M_L$ (dNm)	$M_H$ (dNm)	$V = \frac{M_H - M_L}{t_{90} - t_2}$ (dNm/min)
E100C0	2.34	14.34	1.44	10.26	0.73
Q100C0	0.48	2.78	1.01	17.49	7.18
E100C9	1.90	13.69	1.76	12.02	0.87
Q100C9	0.46	2.01	3.86	18.88	9.81
Q70E30C0	0.60	8.35	1.23	16.33	1.94
Q70E30C9	0.70	9.54	2.65	16.91	1.61

$t_2$  scorch time,  $t_{90}$  optimum cure time,  $M_L$  minimum torque,  $M_H$  maximum torque,  $V$  cure rate

formation at this region of test resulting from the agglomeration of nanoclay particles. For the samples based on Q70E30, the plateau region disappears, which is an indication of good dispersion of nanoclay in the blends.

The cure properties were studied at 160 °C for 20 min using RPA. Rheometry curves and cure parameters of the nanocomposites such as scorch time ( $t_2$ ), optimum cure time ( $t_{90}$ ), maximum torque ( $M_H$ ) and cure rate ( $V$ ) of the samples are shown in Fig. 1b and Table 2, respectively. It may be seen that E100C0 and Q100C9 have the longest and the shortest scorch time, respectively, and the pure EPDM does not achieve the optimum cure by 20 min. Furthermore, after adding the nanoclay to EPDM (E100C9), normally, because of the compatibility between non-polar rubber molecular chains and Cloisite 15A,  $M_H$  increases though  $V$  does not show any variation. These curing behaviors show that the curing rate of silicone rubber is ten times more than that of EPDM containing 1 phr of DCP, with a higher value of  $V$ .

As expected, by adding EPDM to the nanocomposites,  $t_2$  and  $t_{90}$  of the samples increased and cure rate decreased. The presence of Cloisite 15A in the blends increased both  $t_2$  and  $t_{90}$ . In addition, the EPDM phase plays the role of a toughening phase in the blends. Moreover, as a result of compatibility between EPDM and nano-layered silica, Cloisite 15A moves towards the EPDM phase and improves the elasticity of this phase. For this reason, it is expected that in the blends, dispersion of the EPDM phase in the SR matrix would be improved and consequently droplet-matrix morphologies are obtained.

Figure 1b shows that,  $M_H$  of E100C0 is the lowest among those of other samples and the highest  $M_H$  belongs to Q100C9. The  $M_H$  is related to their cross-link density and the interaction between rubber chains and nanoclay. Therefore, the cure behavior demonstrates that there is not a significant variation in cross-link density of EPDM and SR-based nanocomposites in presence of 1 phr DCP and 9 phr of Cloisite 15A. Due to the immigration of nanoclay into the EPDM phase,  $M_H$  and  $V$  of Q70E30C9 sample do not change significantly in comparison with those of Q70E30C0.

## Surface tension of the nanocomposites

For predicting the location of Cloisite 15A particles in the samples, the wetting coefficient ( $\omega$ ) according to the Young's equation can be used [1, 29]:

$$\omega = \frac{\gamma_{\text{organoclay-A}} - \gamma_{\text{organoclay-B}}}{\gamma_{A-B}}, \quad (5)$$

where,  $\gamma_{\text{organoclay-A}}$  and  $\gamma_{\text{organoclay-B}}$  are the interfacial energies between organoclay/polymers  $A$  and  $B$  and  $\gamma_{A-B}$  is the interfacial energy between polymer  $A$  and polymer  $B$ . When  $\omega > 1$ , the organoclay tends to be situated in polymer  $B$  and at  $\omega < -1$ , it will distribute in polymer  $A$ . When  $-1 < \omega < 1$ , the organoclay will be located at the interface of these two phases.

Surface tensions of two rubbers and nanoclay and interfacial tensions between the components are reported in Table 3. EPDM and SR are assigned as polymer  $A$  and polymer  $B$ , respectively. The values of wetting coefficients were obtained as  $-1.9$  using the geometric mean equation and  $-1.7$  by Wu harmonic mean equation. By considering the wetting coefficient data, it was predictable that nanoclay could locate in EPDM phase. This phenomenon resulted in EPDM phase to become hard and affected the morphology of the nanocomposites.

## Fracture surface morphology

Figure 2 compares the SEM micrographs of Q100C9, E100C9, Q70E30C9 and Q70E30C0 samples. As it is evident in this figure, nanoclay is effectively dispersed and an exfoliated morphology is achieved in the EPDM phase because of good compatibility between Cloisite 15A (2M2HT<sup>1</sup>) surfactant and rubber chains. Therefore, through blending, Cloisite 15A moves into EPDM phase and consequently increases the elasticity of this phase owing to the higher filler–rubber interaction. On the other hand, the difference between the polarity of Cloisite 15A and SR causes

<sup>1</sup> Dimethyl, dehydrogenated, tallow quaternary ammonium chloride.

**Table 3** Surface and interfacial tensions calculated from the geometric and Wu harmonic mean equations

Material	Surface tension at 20 °C (mJ/m <sup>2</sup> )		-dγ/dT (mJ/m <sup>2</sup> °C) <sup>a</sup>	References	Surface tension at 50 °C (mJ/m <sup>2</sup> )		Calculated interfacial tension (mN/m)	Wu harmonic mean equation
	γ <sup>p</sup>	γ <sup>i</sup>			γ <sup>p</sup>	γ <sup>i</sup>		
EPDM	5.8	29.7	0.067	[34]	5.47	28.02	γ <sub>EC</sub> <sup>b</sup> = 0.768	γ <sub>EC</sub> = 1.5
SR (PDMS)	1.3	19.2	0.048	[35]	1.22	17.84	γ <sub>SC</sub> <sup>c</sup> = 0.827	γ <sub>SC</sub> = 9.912
Cloisite 15A	11.06	31.47	0.1	[30]	10.29	29.25	γ <sub>ES</sub> <sup>d</sup> = 2.660	γ <sub>ES</sub> = 4.96

<sup>a</sup> Temperature coefficient<sup>b</sup> Interfacial tension between EPDM and Cloisite 15A<sup>c</sup> Interfacial tension between SR and Cloisite 15A<sup>d</sup> Interfacial tension between EPDM and SR

the agglomeration of nanoclay particles. Comparison between Fig. 2a, b specifies inconsistency and compatibility of Cloisite 15A with SR and EPDM, respectively.

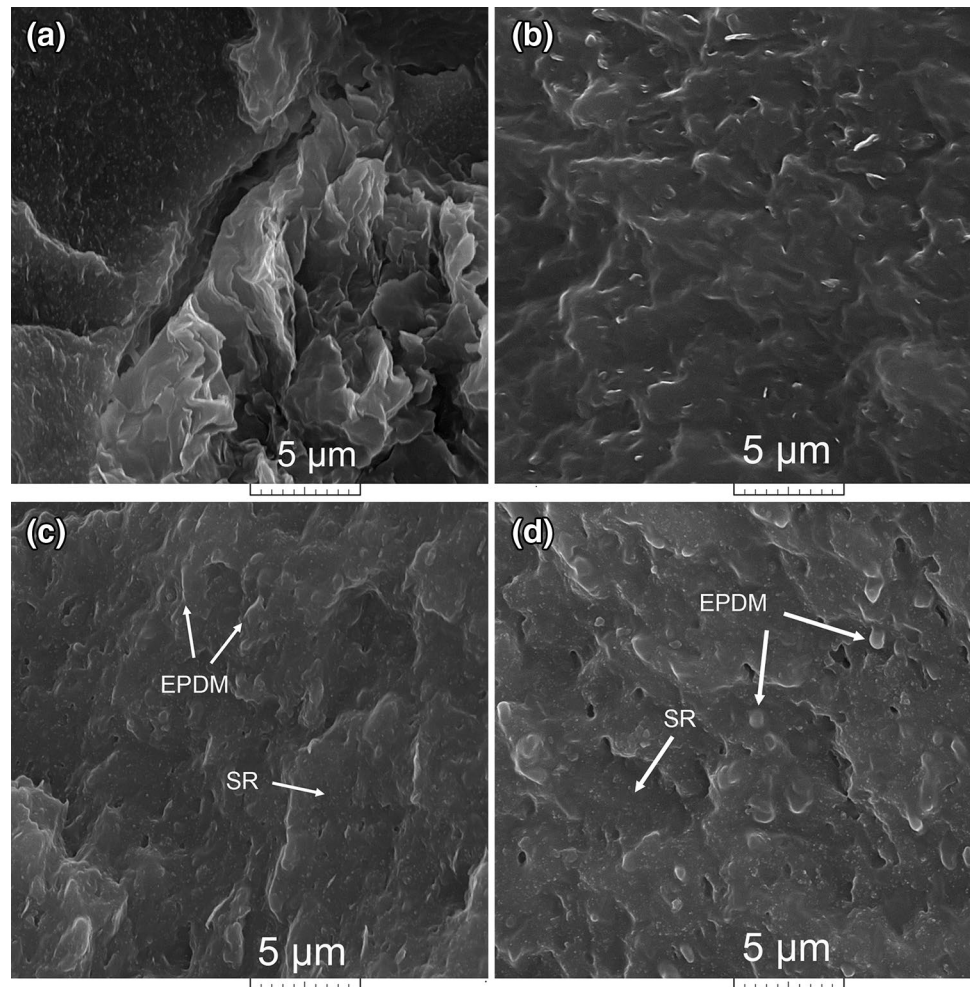
As shown in Fig. 3c, d, the morphology of EPDM/SR blend (Q70E30C0) is a droplet-matrix structure and it displays a good distribution of EPDM in the SR matrix. By adding nanoclay into the blend (Q70E30C9) a fine dispersion of EPDM in the SR matrix is observed. It can be concluded that stabilization mechanism of the blend by nanoclay is accompanied by reduction in interfacial tension, whereas nanoclay as a rigid layer which prevents the coalescence of the dispersed droplets and provides steric hindrance [36, 37]. Moreover, the spherical droplets of EPDM stretched out to oval-shape could be explained by viscosity ratio and elasticity of the phases. Due to the existence of nanoclay in the two phases and subsequent fall in viscosity ratio, the morphology develops toward a co-continuous structure. In addition, entrapment of nanoclay in EPDM, due to their strong interactions, resulted in higher elasticity of this phase, and reduced the shape relaxation of the droplets and stabilized the oval-shaped droplets. Therefore, nanoclay can have a compatibilizing effect on nanocomposites [38].

To confirm nanoclay distribution its related histograms were acquire d by EDX analysis using Image J software (Fig. 3). A histogram is a display of statistical information to show the frequency of data in successive numerical intervals with equal size. Aluminum was detected in EDX analysis, because Si was the prominent element of the SR main chain and it was impossible to distinguish the nanoclay particles in it. It is obvious from Fig. 2a that the fracture surface morphology of Q100C9 due to the agglomeration of nanoclay of its non-polar structure of Cloisite 15A against the polar structure of SR is not homogeneous and has a constricted structure. The EDX analysis (Fig. 3a) also confirms the agglomeration of nanoclay in the SR matrix. Distribution histogram of Q100C9 shows a very vast range of particular distance and it verifies the absence of homogeneous dispersion of the particles as it has appeared in the EDX images. Furthermore, two peaks are emerged in the curve; one in short distance which is related to the agglomerated particles and the other of long distance between different agglomerated clusters.

The homogeneous distribution of nanoclay in EPDM (Fig. 3b), confirmed by EDX analysis, was due to the non-polar structure of both Cloisite 15A and the polymer matrix, which led to even distribution of nanoclay. In addition, symmetrical distribution in the histogram and narrow range of particular distance demonstrated a uniform dispersion of nanoclay in the elastomer matrix.

In addition, the XRD patterns of samples confirmed the location of Cloisite 15A in nanocomposites and were in agreement with the SEM micrographs and EDX images. The XRD patterns of nanocomposites of E100C9, Q100C9,

**Fig. 2** SEM micrographs of **a** Q100C9; **b** E100C9; **c** Q70E30C9; and **d** Q70E30C0



Q70E30C9 and Cloisite15A shown in Fig. 4 illustrate that the Cloisite 15A exhibits an intensive peak at around  $2\theta = 2.7^\circ$ , corresponding to a basal plane spacing ( $d_{001}$ ) of  $32.1 \text{ \AA}$ . In a pattern related to Q100C9, the diffraction peak remains almost in the same position of the neat clay with slight broadening, implying that the clay is not able to disperse in SR effectively. This means that the gallery height of Cloisite 15A has not changed and no intercalated nanostructure is developed in the SR sample, while the diffraction peak of clay in E100C9 has disappeared which might be due to the exfoliated structure within the nanocomposite.

These results may suggest that the clay interacts better with the EPDM than does with the SR in this case. Therefore, it can be predicted that in the EPDM/SR blend nanocomposites, clay is favorably located in the EPDM phase. In Q70E30C9 sample, the intensity of the pattern shows a very broad shoulder and the (001) peak of the clay appears in the same position of neat clay, revealing that the main portion of nanoclay is located in EPDM and it has created a nanostructure exfoliated

morphology and the portion of nanoclay is confined and agglomerated in the SR phase. In Fig. 5, there is a schematic display of nanoclay dispersion in SR, EPDM and SR/EPDM blends.

#### Dynamic mechanical thermal analysis

In this study, dynamic mechanical thermal analysis (DMTA) was performed within the temperature range of  $-160$  to  $100 \text{ }^\circ\text{C}$  in bending mode. The curves of storage modulus ( $E'$ ) and damping factor, ( $\tan \delta$ ) ratio of the loss modulus ( $E''$ ) to the storage modulus, versus temperature are shown in Figs. 6 and 7, respectively.

In the temperature range inspected, there are three zones or states which belong to rubber samples: the first zone is solid in the temperature range of  $-160$  to  $-50 \text{ }^\circ\text{C}$ . At this range the rubbery chains freeze, therefore, they are not able to move and thus the storage modulus of this zone at the starting temperature of the test ( $-160 \text{ }^\circ\text{C}$ ) is dependent on the bulk modulus of material and it is highly affected by stiffness of the chains [39]. As shown in Fig. 6, the storage

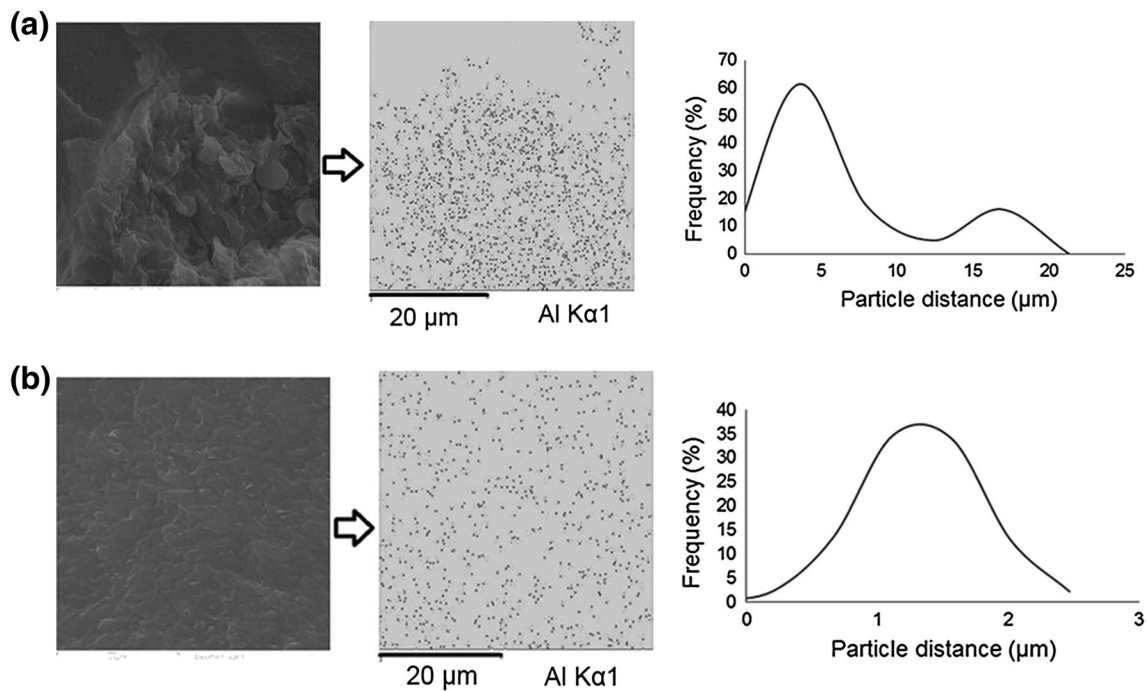


**Fig. 3** EDX images and particles distribution histogram of **a** Q100C9; and **b** E100C9

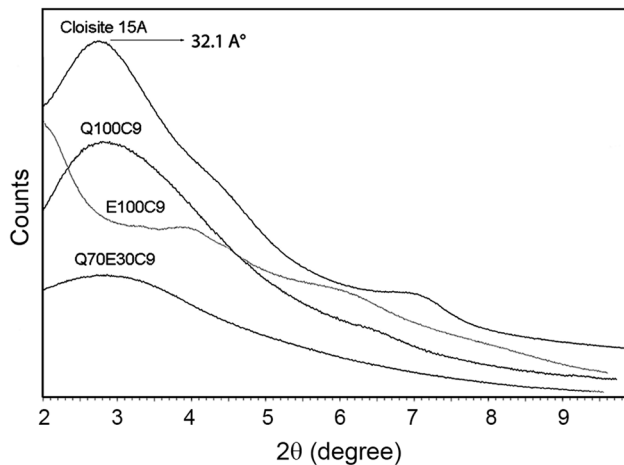


**Fig. 4** XRD patterns of Cloisite 15A, Q100C9, E100C9 and Q70E30C9

modulus of E100C0 and E100C9 samples at  $-160$  °C is very low which is strongly related to the cross-link density of rubber. With implementation of cure rheometry and DMTA curves for EPDM, it is obvious that this rubber would not cure completely and remains as a softening phase in the blends.

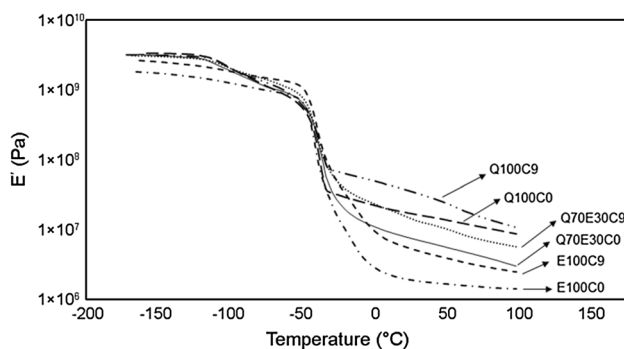
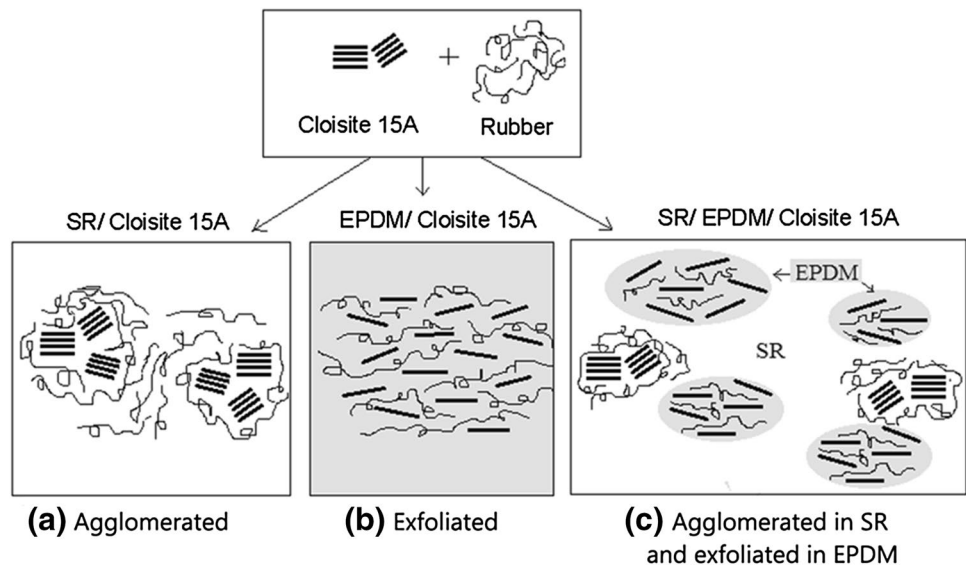
In the second zone, a transition state in the temperature range of  $-50$  to  $0$  °C, the storage modulus of all samples normally decreases with increases in temperature. It may

be notified that the drop in the storage modulus in the transition zone is very noticeable.

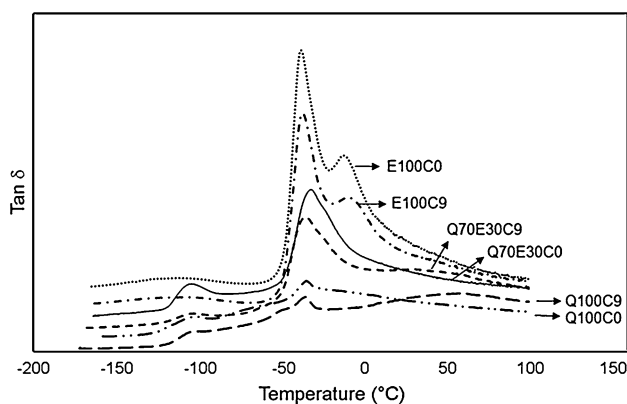
The third zone is in a rubbery state within the temperature range  $0$ – $100$  °C. As it is expected, in the samples containing nanoclay the storage modulus increases in all three zones. This increase becomes more significant in the rubbery zone because of greater interactions between the polymer chains and nanoclay. The  $E'$  values of Q100C9 and E100C0 samples are found at maximum for the former and at minimum for the latter. The downward trend of  $E'$  in the rubbery zone is steeper for nanoclay-containing nanocomposites than that of polymer blends. This can be due to two mechanisms. First, there is a possibility of agglomeration of nanoclay particles in the SR-containing samples as a result of incompatibility of SR with Cloisite 15A. Interactions between these agglomerates are of plastic nature (irreversible motion) and act like a dashpot. Second, nanoclay particles may affect curing mechanisms by peroxide delayed action of Cloisite 15A surfactant which leads to lower elasticity.

Figure 7 presents damping factor or loss tangent ( $\tan \delta$ ) of silicone rubber comprised of two peaks: one at about  $-103$  °C due to its glass transition temperature which is related to the Brownian motion of the main chain and its associated relaxation, and the latter of about  $-35$  °C corresponds to its crystalline melting point [40]. As shown in this figure, the low values of damping factor in SR indicate that this rubber is cured completely in the presence of

**Fig. 5** Schematic presentation of nanoclay dispersion in SR, EPDM and SR/EPDM blends



**Fig. 6** Variation of storage modulus versus temperature in nanocomposites



**Fig. 7** Variation of  $\tan \delta$  versus temperature in nanocomposites

1 phr of DCP and also show a highly elastic behavior after curing the rubber. The comparison between  $\tan \delta$  values of Q100C0 and Q100C9 does not represent a significant

change in temperature or intensity because of the agglomeration of nanoclays in the absence of a strong rubber–filler interaction (Fig. 7).

On the other hand, the larger values of  $\tan \delta$  for E100C0 and E100C9 samples reflect the segmental movements of rubber chains due to an insufficient cross-link density of EPDM after curing. The position of the peaks do not seem to have changed for EPDM-based samples, though the values of  $\tan \delta$  peaks drop for E100C9, implying that the rubber–filler interactions has occurred and thus the movements of the rubber chains have become more restricted. Generally,  $\tan \delta$  peaks involve both segmental motion of the polymer chain in amorphous and crystalline regions. As a result of polymer–filler interactions in the composite, the presence of rigid bodies reduces polymer chain mobility by restricting the side group rotations as well as the motions of polymer backbone [41]. This behavior is evident by reduction in  $\tan \delta$  peak amplitude of E100C9 compared to E100C0.

Both  $\tan \delta$  peaks can be attributed to a partial curing of EPDM with 1 phr DCP. As it can be seen in E100C9 curve, the first peak has emerged at about  $-38$  °C which is related to  $T_g$  of the cured EPDM and the second peak at  $-13$  °C may be associated with  $T_g$  of the uncured part of the rubber related hard segments because of high viscosity of EPDM.

The samples based on SR/EPDM blends (Q70E30C0 and Q70E30C9) showed two peaks at the glass transition temperature of SR ( $-103$  °C) and EPDM ( $-38$  °C) which confirmed the immiscibility of two polymers. The lower  $\tan \delta$  value of Q70E30C9 in comparison with Q70E30C0 may be attributed to rubber–filler interaction. Increasing of  $\tan \delta$  in these blends means that SR has been toughened by the addition of EPDM and this phenomenon has become more important after adding Cloisite 15A to the EPDM phase.



**Table 4** Mechanical properties and viscoelastic parameters obtained from Maxwell model

Sample code	Mechanical properties			Maxwell parameters		
	Tensile strength (MPa)	Elongation-at-break (%)	Hardness (Shore A)	$\eta$ (MPa.s)	$E$ (MPa)	$\tau$ (s)
E100C0	1.284	239.56	48.8	0.067454	0.029799	2.2636
E100C3	1.893	262.76	50.8	0.036635	0.020848	1.7572
E100C6	2.475	301.58	52.2	0.022312	0.015767	1.4151
E100C9	2.790	312.43	55.0	0.037779	0.020194	1.8708
Q100C0	5.443	198.23	72.0	0.088647	0.119271	0.7432
Q100C3	5.122	172.17	75.2	0.075461	0.096174	0.7846
Q100C6	4.986	182.90	78.9	0.080944	0.294431	0.2749
Q100C9	5.160	191.12	79.4	0.081380	0.252767	0.3219
Q90E10C0	5.382	196.24	68.7	0.093219	0.127943	0.7285
Q90E10C3	5.416	229.53	72.0	0.087080	0.141203	0.6167
Q90E10C6	4.939	188.50	72.4	0.085792	0.139696	0.6141
Q90E10C9	4.741	189.93	73.6	0.104630	0.307234	0.3405
Q80E20C0	5.067	199.30	64.4	0.057611	0.040885	1.4090
Q80E20C3	4.465	194.32	66.7	0.053795	0.061388	0.8763
Q80E20C6	4.221	183.25	68.5	0.053765	0.073949	0.7270
Q80E20C9	4.042	190.02	70.6	0.052298	0.276413	0.1892
Q70E30C0	4.337	187.04	62.7	0.024596	0.015781	1.5585
Q70E30C3	3.617	169.43	65.2	0.114156	0.100627	1.1344
Q70E30C6	4.595	225.99	65.1	0.064949	0.079352	0.8184
Q70E30C9	4.462	214.41	66.4	0.125946	0.165066	0.7630

## Mechanical properties

Tensile strength, elongation-at-break and hardness data of nanocomposites are listed in Table 4. As it can be seen, hardness is normally increased with increasing the nanoclay content in all nanocomposites. At higher EPDM ratio in SR/EPDM blends the mechanical properties are weaker due to lower mechanical strength of EPDM and immiscibility of the elastomers. In E100C0 to E100C9 samples, there is a smooth rise in mechanical properties due to increasing Cloisite 15A content. This may imply that the nanoclay dispersion has improved well in EPDM phase and consequently it has a positive effect on the tensile strength, elongation-at-break and hardness of nanocomposites through rubber–filler interactions.

Based on the morphological studies presented in previous sections, it was confirmed that exfoliation of Cloisite 15A in EPDM did occur. On the other hand, agglomeration of nanoclay in SR led to greater hardness but it also showed a negligible variation in tensile strength and elongation-at-break because of the lowest level of rubber–filler interactions in SR (from Q100C0 to Q100C9). It was, however, expected that by the presence of nanoclay in the EPDM phase, lower viscosity and higher wettability of SR would induce dispersion of some parts of nanoclay layers in the SR phase. In addition, in case of nanocomposites

containing 10 and 20 % EPDM, the final properties of samples were mostly dependent on the behavior of nanoclay in the SR matrix due to their low EPDM content. However, increasing the content ratio of EPDM and nanoclay in the samples could lead to improved mechanical strength.

## Prediction of viscoelastic parameters using Maxwell model

In this study,  $E$  and  $\eta$  were obtained using the Maxwell model from experimental data at the initial time of deformation (less than 1.5 s as represented in Fig. 8). For this purpose, the viscoelastic parameters ( $E$  and  $\eta$ ) were calculated from data and then replaced in the Maxwell equation.

The theoretical equations were derived from the Maxwell model and used for all the samples as follows:

Rearrangement of Eq. (4) by substitution of and gives:

$$B = \frac{1}{\eta} \quad A = \frac{1}{E}$$

$$d\varepsilon = A d\sigma + B \sigma dt. \quad (6)$$

At the early stage of deformation, it may be assumed that the stress-time curve is linear. Therefore, by assumption of Eq. (6) it may be written as:  $\sigma = \alpha t$ ,

$$d\varepsilon = A d\sigma + \frac{B}{\alpha} \sigma d\sigma, \quad (7)$$

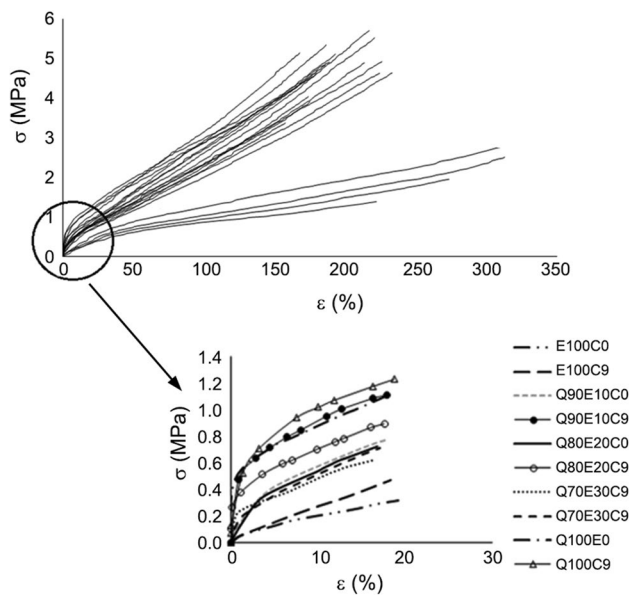


**Fig. 8** Stress–strain curves of the nanocomposites at the initial zone of test

Integration of Eq. (7) gives:

$$\varepsilon = A\sigma + \frac{B}{2\alpha}\sigma^2, \tag{8}$$

Equation (8) can be written as:

$$a\varepsilon = \sigma^2 + b\sigma, \tag{9}$$

where,  $a$  and  $b$  are  $2\alpha\eta$  and  $\frac{2\alpha\eta}{E}$ , respectively. We can rearrange Eq. (9) to obtain Eq. (10):

$$\sigma = \left( a\varepsilon + \frac{b^2}{4} \right)^{1/2} - \frac{b}{2}. \tag{10}$$

Figure 9 depicts the stress–strain curves for the experimental data and Maxwell model, and Table 4 specifies the viscoelastic parameters ( $E$  and  $\eta$ ) calculated by the Maxwell model. It is obvious that at initial time of the tensile test the rubber–filler interaction can control the stress–strain behavior of the samples. In the EPDM-based samples, (from E100C0 to E100C9), a high- accuracy fitting is not provided because of the incomplete vulcanization

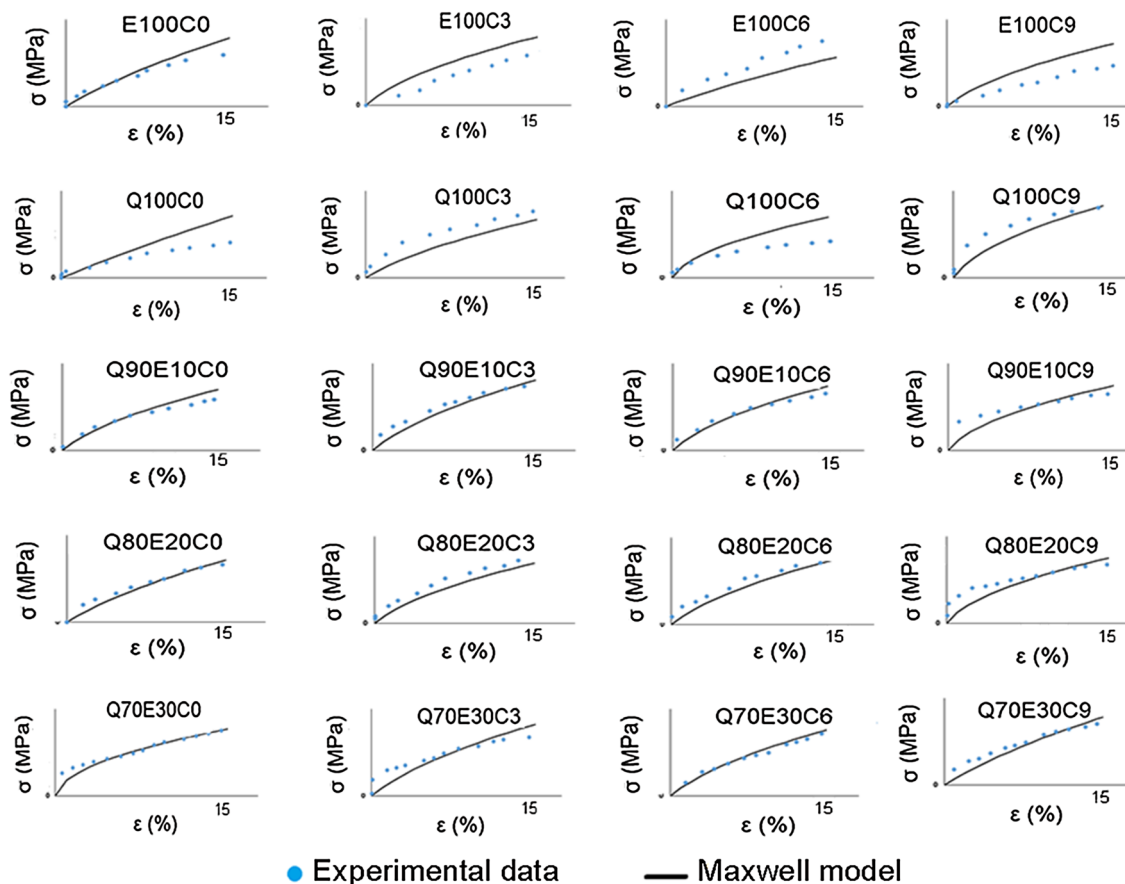


**Fig. 9** Stress–strain curves obtained from experimental data and Maxwell model

by 1 phr DCP. Also, in SR-based samples, (from Q100C0 to Q100C9), the poor rubber–filler interaction does not allow good fitting between the experimental and calculated data because of the agglomeration of nanoclay particles in the SR matrix. On the other hand, in those nanocomposites based on SR/EPDM, there is good fitting between the model and the experimental data. This stress–strain behavior in the blends shows that at higher nanoclay contents, a better matching in viscoelastic behavior of two immiscible rubbers is easily obtained. In other words, the advantage of nanoclay in the blend is to provide a better matching between the viscosities of SR and EPDM rubbers.

The third characteristics of the Maxwell model as it is listed in Table 4 is the relaxation time ( $\tau = \eta/E$ ). This property in EPDM- and SR-based samples, does not display a regular trend because of partial curing of the EPDM-based samples and filler flocculation in SR-based samples because of poor rubber–filler interaction. Nonetheless, after blending, the nanoclay layers are mostly located in EPDM phase and an increase in rubber–filler interactions occurs, thus the elasticity of EPDM phase is improved. Therefore, a fall in relaxation time of the samples occurs after adding the nanoclay into the blend. As it is obvious, in the blends with high EPDM content (Q70E30C0 to Q70E30C9), the variations in relaxation time are significant because with increasing the elasticity of EPDM phase the relaxation time drops. Based on the observations made earlier the SEM micrographs and EDX analysis of the blends showed that, with higher content of EPDM phase, the circular-droplet morphology transformed to oval-shape morphology. This could be due to the migration of Cloisite 15A into the EPDM phase and good rubber–filler interaction, resulting in a better coherency between the droplets in the matrix.

## Conclusion

In summary, SR/EPDM nanocomposites were prepared having an organically modified clay (Cloisite 15A) using melt blending method. Cure properties showed a high cure rate difference between the SR and EPDM and incomplete cross-linking of EPDM. Calculating the wetting coefficients of the nanocomposites predicted the tendency of nanoclay to be located in the EPDM phase due to the compatibility of rubber chains and nanoclay surfactants and strong rubber–filler interactions. SEM micrographs demonstrated a homogeneous distribution of the nanoclay particles in EPDM and their agglomeration in SR, which was also confirmed by EDX analysis. The migration of nanoclay into the EPDM phase in the blends changed the droplet structure in this phase to oval-shape because of increasing EPDM elasticity. The XRD results revealed the exfoliation of nanoclay in the EPDM phase; however,

the intergallery spacing of nanoclay did not change in the SR matrix. Immiscibility of these two elastomers was evident by observation of the DMTA results, because two  $\tan \delta$  peaks ( $T_g$ ) belonged to the blends and nanocomposites appeared on the glass transition temperature of each elastomer. Exfoliation of nanoclay in the EPDM-based nanocomposites led to improved mechanical properties but the agglomeration of nanoclay in the SR-based nanocomposites led to weaker mechanical properties. By increasing the EPDM ratio in the blends, there was a depression in the mechanical strength, but high content of EPDM accompanied by high amount of nanoclay improved the mechanical strength. By addition of the clay to SR/EPDM blends, the viscoelastic behavior of these elastomers displayed close similarity to each other and hence a good fitting between the experimental data and Maxwell model was achieved.

## References

1. Das A, Mahaling R, Stöckelhuber K, Heinrich G (2011) Reinforcement and migration of nanoclay in polychloroprene/ethylene–propylene–diene–monomer rubber blends. *Compos Sci Technol* 71:276–281
2. Krajnc M, Karger Kocsis J, Sebenik U (2013) Grafting of maleic anhydride onto an ethylene–propylene–diene terpolymer and concurrent organoclay nanocomposite preparation in solution and melt. *J Appl Polym Sci* 127:950–958
3. Ebadi Dehaghani H, Khonakdar HA, Barikani M, Jafari SH (2015) Experimental and theoretical analyses of mechanical properties of PP/PLA/clay nanocomposites. *Compos Part B Eng* 69:133–144
4. Le Baron PC, Wang Z, Pinnavaia TJ (1999) Polymer-layered silicate nanocomposites: an overview. *Appl Clay Sci* 15:11–29
5. Ma J, Yu ZZ, Kuan HC, Dasari A, Mai YW (2005) A new strategy to exfoliate silicone rubber/clay nanocomposites. *Macromol Rapid Commun* 26:830–833
6. Chang YW, Yang Y, Ryu S, Nah C (2002) Preparation and properties of EPDM/organomontmorillonite hybrid nanocomposites. *Polym Int* 51:319–324
7. Sinha Ray S, Okamoto M (2003) Polymer/layered silicate nanocomposites: a review from preparation to processing. *Prog Polym Sci* 28:1539–1641
8. Kang D, Kim D, Yoon SH, Kim D, Barry C, Mead J (2007) Properties and dispersion of EPDM/modified-organoclay nanocomposites. *Macromol Mater Eng* 292:329–338
9. Ghasemi I, Karrabi M, Mohammadi M, Azizi H (2010) Evaluating the effect of processing conditions and organoclay content on the properties of styrene–butadiene rubber/organoclay nanocomposites by response surface methodology. *Express Polym Lett* 4:62–70
10. Rajini V, Deepalaxmi R (2012) Property modification of SiR-EPDM blends by electron beam irradiation. In: 2012 IEEE international conference on condition monitoring and diagnosis (CMD), pp 1071–1076. doi:10.1109/CMD.2012.6416342
11. Bagheri Kazemabad S, Khavandi A, Chen B (2012) Evaluation of toughening mechanisms of polypropylene/ethylene–octene copolymer/maleic anhydride-grafted poly (ethylene-co-octene)/clay nanocomposite. *Polym Int* 62:566–572
12. Ock HG, Kim DH, Ahn KH, Lee SJ, Maia JM (2016) Effect of organoclay as a compatibilizer in poly (lactic acid) and natural rubber blends. *Eur Polym J* 76:216–227

13. Acharya H, Kumar Srivastava S (2014) EPDM/silicone blend layered silicate nanocomposite by solution intercalation method: morphology and properties. *Polym Compos* 35:1834–1841
14. Li Y, Shimizu H (2004) Novel morphologies of poly (phenylene oxide)(PPO)/polyamide 6 (PA6) blend nanocomposites. *Polymer* 45:7381–7388
15. Asaad JN, El-Nashar DE, Mansour SH (2014) Effect of modified clay and Mg (OH)<sub>2</sub> on the properties of ethylene propylene diene monomer/silicon rubber nanocomposites. *Proc Int Mech Eng NJ Nano* 229:121–130
16. Sengupta R, Chakraborty S, Bandyopadhyay S, Dasgupta S, Mukhopadhyay R, Auddy K, Deuri A (2007) A short review on rubber/clay nanocomposites with emphasis on mechanical properties. *Polym Eng Sci* 47:1956–1974
17. Maiti M, Bhattacharya M, Bhowmick AK (2008) Elastomer nanocomposites. *Rubber Chem Technol* 81:384–469
18. Pasbakhsh P, Ismail H, Fauzi MA, Bakar AA (2009) Influence of maleic anhydride grafted ethylene propylene diene monomer (MAH-g-EPDM) on the properties of EPDM nanocomposites reinforced by halloysite nanotubes. *Polym Test* 28:548–559
19. Ehsani M, Borsi H, Gockenbach E, Morshedian J, Bakhshandeh G (2004) An investigation of dynamic mechanical, thermal, and electrical properties of housing materials for outdoor polymeric insulators. *Eur Polym J* 40:2495–2503
20. Mansor NS, Hamzah MS, Kamarol M, Mariatti MA (2014) Comparative study of dielectric strength between SiR/EPDM and PP/EPDM blends with various type of nanofillers. *Adv Mater Res* 832:483–487
21. Dang ZM, Xia YJ, Zha JW, Yuan JK, Bai J (2011) Preparation and dielectric properties of surface modified TiO<sub>2</sub>/silicone rubber nanocomposites. *Mater Lett* 65:3430–3432
22. Jung SY, Kim BK (2009) Preparation and characteristics of high voltage liquid silicone rubber by modified cross-linking agent. *Trans Electr Electron Mater* 10:9–15
23. Kole S, Srivastava S, Tripathy D, Bhowmick A (1994) Accelerated hydrothermal weathering of silicone rubber, EPDM, and their blends. *J Appl Polym Sci* 54:1329–1337
24. Yang L, Hu Y, Lu H, Song L (2006) Morphology, thermal, and mechanical properties of flame-retardant silicone rubber/montmorillonite nanocomposites. *J Appl Polym Sci* 99:3275–3280
25. Raja Prabu R, Udayakumar K, Abdullah Khan M, Abdul Majeed S (2007) Electrical insulation characteristics of silicone and EPDM polymeric blends. I. *IEEE Trans Dielectr Electr Insul* 14:1207–1214
26. Kole S, Chaki T, Bhowmick AK, Tripathy D (1993) Effect of compatibiliser, curing sequence and ageing on the thermal stability of silicone rubber, EPDM rubber and their blends. *Polym Degrad Stabil* 41:109–116
27. Xu G, Qin S, Yu J, Huang Y, Zhang M, Ruan W (2015) Effect of migration of layered nanoparticles during melt blending on the phase morphology of poly (ethylene terephthalate)/polyamide 6/montmorillonite ternary nanocomposites. *RSC Adv* 5:29924–29930
28. Zhang C, Pal K, Byeon JU, Han SM, Kim JK (2011) A study on mechanical and thermal properties of silicone rubber/EPDM damping materials. *J Appl Polym Sci* 119:2737–2741
29. Bagheri Kazemabad S, Fox D, Chen Y, Geever LM, Khavandi A, Bagheri R, Higginbotham CL, Zhang H, Chen B (2012) Morphology, rheology and mechanical properties of polypropylene/ethylene–octene copolymer/clay nanocomposites: effects of the compatibilizer. *Compos Sci Technol* 72:1697–1704
30. Kooshki RM, Ghasemi I, Karrabi M, Azizi H (2013) Nanocomposites based on polycarbonate/poly (butylene terephthalate) blends effects of distribution and type of nanoclay on morphological behavior. *J Vinyl Addit Technol* 19:203–212
31. Li Y, Wei GX, Sue HJ (2002) Morphology and toughening mechanisms in clay-modified styrene-butadiene-styrene rubber-toughened polypropylene. *J Mater Sci* 37:2447–2459
32. Mirabedini AS, Karrabi M, Ghasemi I (2013) Viscoelastic behavior of NBR/phenolic compounds. *Iran Polym J* 22:25–32
33. Fried JR (2005) Polymer science and technology. In: *Viscoelasticity and rubber elasticity*, 2nd edn. Prentice Hall, New Delhi
34. Bonnerup C, Gatenholm P (1993) The effect of surface energetics and molecular interdiffusion on adhesion in multicomponent polymer systems. *J Adhes Sci Technol* 7:247–262
35. Roe RJ (1965) Parachor and surface tension of amorphous polymers. *J Phys Chem* 69:2809–2810
36. Fenouillot F, Cassagnau P, Majeste JC (2009) Uneven distribution of nanoparticles in immiscible fluids: morphology development in polymer blends. *Polymer* 50:1333–1350
37. Elias L, Fenouillot F, Majesté JC, Martin G, Cassagnau P (2008) Migration of nanosilica particles in polymer blends. *J Polym Sci Pol Phys* 46:1976–1983
38. Van Puyvelde P, Moldenaers P (2005) Rheology and morphology development in immiscible polymer blends. *Rheology Rev* 2005:101
39. Song K, Zhang Y, Meng J, Minus ML (2015) Spectral analysis of lamellae evolution and constraining effects aided by nano-carbons: a coupled experimental and simulation study. *Polymer* 75:187–198
40. Kole S, Bhattacharya A, Tripathy D, Bhowmick AK (1993) Influence of curative, filler, compatibilizer, domain size, and blend ratio on the dynamic mechanical properties of silicone–EPDM blends. *J Appl Polym Sci* 48:529–545
41. Song K, Zhang Y, Minus ML (2015) Polymer interphase self-reinforcement and strengthening mechanisms in low-loaded nanocomposite fibers. *Macromol Chem Phys* 216:1313–1320